

Spin pumping into two-dimensional electron systems

Takuya Inoue,¹ Gerrit E. W. Bauer,^{1,2,3} and Kentaro Nomura¹

¹*Institute for Materials Research, Tohoku University, Sendai 980-8577, Japan*

²*Kavli Institute of NanoScience, TU Delft Lorentzweg 1, 2628 CJ Delft, The Netherlands*

³*WPI-AIMR, Tohoku University, Sendai 980-8577, Japan*

(Dated: October 3, 2016)

We study the spin current injected by spin pumping into single layer graphene and the two-dimensional electron gas (2DEG) with ferromagnetic contacts using scattering theory. The spin currents pumped into graphene are very distinct from that into the 2DEG since importantly affected by Klein tunneling.

PACS numbers:

I. INTRODUCTION

Spintronics takes advantage of both the charge and spin degrees of freedom of the electron to generate novel device functionalities for information and communication technologies. Key concepts in spintronics are the spin current, i.e. net flows of spin angular momentum, and the spin accumulation, i.e. a non-equilibrium imbalance between the densities of the two spin species. Both can be generated in non-magnetic conductors by several methods, such as electrical^{1,2}, optical³, and thermal spin injection⁴ and the spin-orbit interaction⁵. It is also possible to inject spins dynamically into various non-magnetic conductors by “pumping” via a ferromagnetic contact with a time-dependent magnetization. The effect can be understood in terms of adiabatic quantum pumping, i.e. the generation of a current not by an applied voltage but a time-periodic modulation of the scattering matrix by external parameters. Spin pumping does not suffer from the conductance mismatch problem that plagues electrical spin injection^{6,7} and is at the root of many physical phenomena, e.g. the spin Seebeck effect⁸. Here we report a theoretical study on spin pumping into two-dimensional electronic systems, such as the two-dimensional electron gas (2DEG) in layered semiconductors and graphene.

A 2DEG system may be formed at the interface between two different semiconductors, such as modulation-doped GaAs/AlGaAs heterojunctions or quantum wells that at low temperatures support electron mobilities of $> 10^7 \text{ cm}^2 \text{ V}^{-1} \text{ s}^{-1}$ corresponding to transport mean-free paths of $\approx 100 \mu\text{m}$ ⁹. While spin injection into thin semiconductor layers has been reported¹⁰, we are not aware of spin injection experiments into high-mobility 2DEGs, presumably due to the conductance mismatch problem.

Monatomic layers such as graphene and transition metal dichalcogenides also have two-dimensional electronic structures^{11–14} and are interesting candidates for spintronic applications^{16–18}. For graphene high electronic mobilities of $3.5 \times 10^5 \text{ cm}^2 \text{ V}^{-1} \text{ s}^{-1}$ have been reported¹⁹. Electric spin injection has been achieved with long spin flip diffusion lengths of $13/24 \mu\text{m}$ at room temperature/4 K, respectively²⁰. The low-energy excitations of graphene close to the charge-neutral Fermi energy are well described by the massless-Dirac equation²¹ and to transport properties very different from those of 2DEGs.

Recently, experiments on ferromagnetic resonance (FMR) of permalloy (Py) on graphene report enhancement of the intrinsic resonance line widths and non-local voltages^{13,22,23}. These experiments are interpreted as evidence for spin currents pumped into graphene^{24–27}. Spin pumping can be formulated^{24–26} as a spin-dependent generalization of the Büttiker-Brouwer adiabatic quantum pumping formula based on the scattering theory of transport²⁸. Rahimi and Moghaddam²⁹ computed spin pumping into graphene by a magnetic insulator, which has the advantage that parallel conductance channels that may exist for magnetic metals are completely suppressed. Recently, transport experiments of graphene on a magnetic insulator Yttrium Iron Garnet (YIG) substrate have been reported^{30,31} that show an induced proximity exchange splitting of $\sim 0.1 \text{ T}$ in the graphene electronic structure³¹. Much larger exchange splittings have been predicted for graphene on EuO ³² and observed for graphene/ EuS ³³. We note that spin pumping into 2D systems by an electrically insulating magnetic gate may efficiently emulate the spin pumping and maser action predicted to occur by inhomogeneous Zeeman fields^{34,35}.

Here we consider a ferromagnetic insulator (FI) on top of a two-dimensional electron system (2DEG or graphene) connected to electron reservoirs as in Fig 1, where the latter are kept at the same chemical potential. An additional metallic gate on top of the FI tunes the electron density and Fermi energy of the electrons relative to that in the reservoirs. The exchange interaction of the conduction electrons with the ferromagnet induces a proximity exchange potential that weakly magnetizes the electron gas^{31,36,37}. When the FI magnetization moves sufficiently slowly, e.g. under FMR, the induced magnetization follows adiabatically. The scattering matrix connecting the reservoirs changes parametrically in time, thereby pumping a spin current into the reservoirs. The spin coherence length $\lambda = \pi / |k_F^\uparrow - k_F^\downarrow|$, where k_F^σ is the Fermi wave number of the conduction electrons under the ferromagnet with $\sigma = \uparrow$ or \downarrow , is now much larger than that of metallic ferromagnets, in which λ is of the order of a few ångströms. Spin-dependent DC transport in such proximity-magnetized graphene has been studied theoretically^{38,39}. Here we consider the spin pumping of a weakly magnetized ballistic electron gas (2DEG and graphene) with slightly different Fermi circles for up and down spins and a λ that should be larger than the length D of the scattering region.

In the absence of spin-orbit interaction, the scattering matrix for a mono-domain ferromagnetic element sandwiched by two normal metals may be decomposed as

$$S = S^\uparrow \hat{u}^\uparrow + S^\downarrow \hat{u}^\downarrow, \quad (1)$$

where S^σ is the scattering matrix for spins up (down) along \mathbf{m} , the unit vector of magnetization of the ferromagnet. The spin-projected scattering matrix

$$S^\sigma = \begin{pmatrix} r^\sigma & t^\sigma \\ t^\sigma & r^\sigma \end{pmatrix}, \quad (2)$$

where t^σ/r^σ are transmission/reflection coefficient matrices for spin σ . \hat{u}^σ is the projection operator

$$\hat{u}^\sigma = \frac{1}{2}(1 \pm \hat{\mathbf{s}} \cdot \mathbf{m}), \quad (3)$$

where $\hat{\mathbf{s}} = \sum_{l=x,y,z} \hat{s}_l \mathbf{e}_l$ and \hat{s}_l are the Pauli matrices. The spin current pumped into adjacent normal metals then reads

$$\mathbf{I}_{s,R}^{pump} = \frac{\hbar}{4\pi} (g_r \mathbf{m} \times \frac{d\mathbf{m}}{dt} - g_i \frac{d\mathbf{m}}{dt}), \quad (4)$$

where $g = \sum_{nn'} (\delta_{nn'} - r_{nn'}^\dagger (r_{nn'}^\dagger)^*) - t_{nn'}^\dagger (t_{nn'}^\dagger)^*$ is the complex spin-mixing conductance with $\text{Re } g = g_r$, $\text{Im } g = g_i$. We focus here on wide two-dimensional systems with widths W with continuous transport channel index $n \rightarrow k_y = k_F \sin \phi$, where k_F is the Fermi wave number in the leads and ϕ the angle of incidence. In the following we assume a ballistic scattering region; the wave numbers are conserved and all matrices diagonal. Then

$$g = \frac{2k_F W}{\pi} \int_0^\pi d\phi (1 - r^\dagger(\phi)(r^\dagger(\phi))^* - t^\dagger(\phi)(t^\dagger(\phi))^*). \quad (5)$$

The proximity exchange potential of the (single-domain) ferromagnet polarizes the conduction electrons. Under ferromagnetic resonance conditions the magnetization precesses around the z axis $\mathbf{m}(t) = (\sqrt{1-m^2} \cos \omega t, \sqrt{1-m^2} \sin \omega t, m)$ where m is the cosine of the precession cone angle. Then the instantaneous spin current pumped into the adjacent leads reads

$$\mathbf{I}_{s,R}^{pump}(t) = \frac{\hbar \omega}{4\pi} \begin{pmatrix} m \sqrt{1-m^2} g_r \cos \omega t + \sqrt{1-m^2} g_i \sin \omega t \\ m \sqrt{1-m^2} g_r \sin \omega t - \sqrt{1-m^2} g_i \cos \omega t \\ (1-m^2) g_r \end{pmatrix}, \quad (6)$$

while its time average becomes

$$\mathbf{J}_s = \frac{\omega}{2\pi} \int_0^{2\pi} dt \mathbf{I}_s^{pump}(t) = \frac{\hbar \omega}{4\pi} (1-m^2) g_r \mathbf{e}_z. \quad (7)$$

When this spin current is dissipated in the conductor or reservoirs, the loss of angular momentum and energy increases the viscous damping of the magnetization dynamics that is observable as an enhanced broadening of ferromagnetic resonances^{24,25,27}. The spin-current may be converted into a charge signal by metallic contacts that either have a large spin Hall angle⁴⁰ or are ferromagnetic⁶. In the following we focus on the principle of spin current generation, but leave the modeling of the spin current detection for future study.

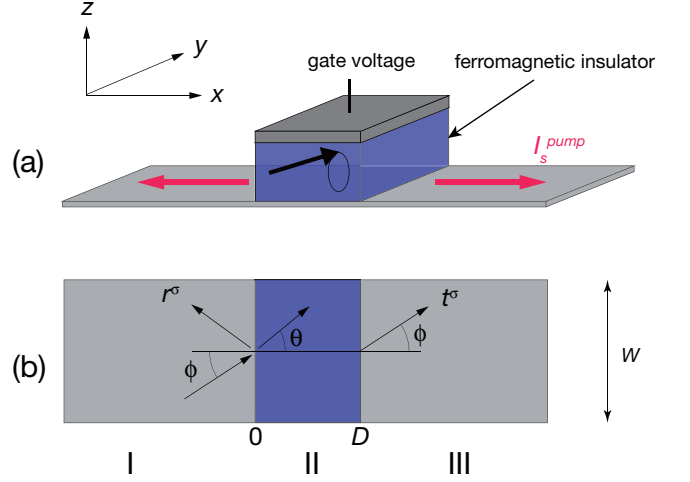


FIG. 1: (a) Schematic of the spin-pumping device: a metallic gate on a ferromagnetic insulator film on top of a 2D electronic system, either a 2DEG or graphene. We calculate reflection and transmission coefficients for electrons impinging on the gated region. (b) ϕ is the angle of incidence and θ the refraction angle. Red arrows represent the spin currents induced by spin pumping.

II. MODEL & RESULTS

We consider Hamiltonians of the form

$$H^{2D} = H_{kin}^{2D} + U(\mathbf{r}, t), \quad (8)$$

where H_{kin}^{2D} is the kinetic energy of the electrons that experience a spin-dependent potential below the FI-gated area:

$$U(\mathbf{r}, t) = V_c - \mathbf{Jm}(t) \cdot \mathbf{s}. \quad (9)$$

V_c is the electric potential controlled by the metal gate and $-\mathbf{Jm}(t) \cdot \mathbf{s}$ is the exchange potential that parametrically depends on the FI magnetization direction \mathbf{m} and electron spin \mathbf{s} . In the absence of more detailed information J is taken to be not depend on V_c . At equilibrium, the magnetization direction $\mathbf{m}_0 \parallel \hat{z}$ is constant and the potential for up (down) spin electrons along the spin quantization \hat{z} -axis reduces to

$$V_\sigma \equiv V_c - \sigma J \quad (10)$$

with $\sigma = \pm 1$ for spin up and down. The spin current per unit width $j_s = J_s/W$ is a function of several parameters:

$$j_s = j_s(E_F, V_c, J, D). \quad (11)$$

Outside the gated region the potential vanishes. Its shape in the intermediate region depends on the device design. Here we consider two limits. When the potential varies slowly on the scale of the electron wave length, an adiabatic approximation is appropriate⁴¹. In this model the potentials changes slowly on the scale of the electron wave length from $V_\sigma^{(slow)}(\mathbf{r}) = 0$ for $x \ll 0$ to $V_\sigma^{(slow)}(\mathbf{r}) = V_\sigma$ for $0 \leq x \leq D$ and then back to $V_\sigma^{(slow)}(\mathbf{r}) = 0$ for $x \gg 0$. In the other limit

the potential at the boundaries of the scattering region changes abruptly (on the scale of the electron wave length):

$$V_{\sigma}^{(\text{abrupt})}(\mathbf{r}) = \begin{cases} 0, & x < 0 \\ V_{\sigma}, & 0 \leq x \leq D \\ 0, & D < x. \end{cases} \quad (12)$$

The scattering at the step potential can be treated by quantum mechanical wave function matching. The reality is likely to be an intermediate between the two extremes and can be understood qualitatively by interpolation.

A. 2DEG

First, we discuss a wide strip of a 2DEG. In the Hamiltonian

$$H_{kin}^{2\text{DEG}} = -\frac{\hbar^2 \nabla^2}{2m^*}, \quad (13)$$

m^* is the effective mass. Assuming sufficiently wide strips we may use the periodic boundary condition in the lateral y -direction. We consider electrons that in the reservoirs are at the Fermi energy $E_F = \hbar^2 k_F^2 / (2m^*)$ with $k_F = \sqrt{k_x^2 + k_y^2}$.

We first discuss the abrupt potential limit in which the Hamiltonian can be written as

$$H^{2\text{DEG}} = -\frac{\hbar^2 \nabla^2}{2m^*} + V_{\sigma}^{(\text{abrupt})}(\mathbf{r}). \quad (14)$$

The electrons in region I ($x < 0$) are a linear combination of incoming and reflected waves (see Figure 1)

$$\psi_{I,\sigma,\mathbf{k}}(\mathbf{r}) = e^{ik_x x + ik_y y} + r^{\sigma} e^{-ik_x x + ik_y y}. \quad (15)$$

In region II ($0 < x < D$)

$$\psi_{II,\sigma,\mathbf{k}}(\mathbf{r}) = a^{\sigma} e^{iq_{x,\mathbf{k}}^{\sigma} x + iq_y^{\sigma} y} + b^{\sigma} e^{-iq_{x,\mathbf{k}}^{\sigma} x + iq_y^{\sigma} y}, \quad (16)$$

and in region III ($x > D$)

$$\psi_{III,\sigma,\mathbf{k}}(\mathbf{r}) = t^{\sigma} e^{ik_x x + ik_y y}, \quad (17)$$

where the indices $i = \{I, II, III\}$, $\sigma = \pm$, and \mathbf{k} denote electrons with spin σ in region i with wave vector $\mathbf{k} = (k_x, k_y)$. $k_x = k_F \cos \phi$ and $k_y = k_F \sin \phi$ are the wave vector components outside the scattering region and kinetic energy $E - V_{\sigma} = \hbar^2 (q_x^2 + q_y^2) / (2m^*)$. The boundary conditions at the potential steps are $\psi_{I,\sigma}(0, y) = \psi_{II,\sigma}(0, y)$, $\psi_{II,\sigma}(D, y) = \psi_{III,\sigma}(D, y)$ and $k_y = q_y^{\sigma}$. Except for the singular point $V_{\sigma} = E - \hbar^2 k_y^2 / (2m^*)$ (or $q_x^{\sigma} = 0$), the transmission and reflection coefficients read

$$t_{\mathbf{k}}^{\sigma} = \frac{2k_x q_{x,\mathbf{k}}^{\sigma} e^{-ik_x D}}{i(k_x^2 + q_x^2) \sin q_{x,\mathbf{k}}^{\sigma} D + 2k_x q_{x,\mathbf{k}}^{\sigma} \cos q_{x,\mathbf{k}}^{\sigma} D} \quad (18)$$

$$r_{\mathbf{k}}^{\sigma} = \frac{i(q_x^2 - k_x^2) \sin q_{x,\mathbf{k}}^{\sigma} D}{i(k_x^2 + q_x^2) \sin q_{x,\mathbf{k}}^{\sigma} D + 2k_x q_{x,\mathbf{k}}^{\sigma} \cos q_{x,\mathbf{k}}^{\sigma} D}. \quad (19)$$

When $E \gg V_{\sigma}$, i.e. when the potential steps are relatively small, **GB**: Can you please check changes?

$$q_x^{\sigma} = \pm \sqrt{\frac{2m^*}{\hbar^2} (E - V_{\sigma}) - q_y^2} \rightarrow \pm \sqrt{\frac{2m^*}{\hbar^2} E - k_y^2} = \pm k_x.$$

Also $q_{x,\mathbf{k}}^{\sigma} \approx \sqrt{-2m^* V_{\sigma}} / \hbar \gg \sqrt{2m^* E} / \hbar = k$ and we obtain the simplified expressions

$$t_{\mathbf{k}}^{\sigma} \cong \frac{2k_F e^{-ikD \cos \phi \cos \phi}}{iq_{x,\mathbf{k}}^{\sigma} \sin q_{x,\mathbf{k}}^{\sigma} D + 2k_F \cos \phi \cos \phi q_{x,\mathbf{k}}^{\sigma} D} \cong \begin{cases} e^{-ik_F D \cos \phi}, & q_{x,\mathbf{k}}^{\sigma} D = 2n\pi \\ -e^{-ik_F D \cos \phi}, & q_{x,\mathbf{k}}^{\sigma} D = (2n+1)\pi \\ 0, & q_{x,\mathbf{k}}^{\sigma} D \neq n\pi \end{cases} \quad (20)$$

$$r_{\mathbf{k}}^{\sigma} \cong \frac{iq_{x,\mathbf{k}}^{\sigma} \sin q_{x,\mathbf{k}}^{\sigma} D}{iq_{x,\mathbf{k}}^{\sigma} \sin q_{x,\mathbf{k}}^{\sigma} D + 2k_F \cos \phi \cos \phi q_{x,\mathbf{k}}^{\sigma} D} \cong \begin{cases} 0, & q_{x,\mathbf{k}}^{\sigma} D = n\pi \\ 1, & q_{x,\mathbf{k}}^{\sigma} D \neq n\pi \end{cases}. \quad (21)$$

For the special point $V_{\sigma} = E - \hbar^2 k_y^2 / (2m^*)$, the transmission and reflection coefficients reduce to

$$t_{\mathbf{k}}^{\sigma} = \frac{-2ie^{-ik_x D}}{ik_x D - 2}, r_{\mathbf{k}}^{\sigma} = \frac{ik_x D}{ik_x D - 2}. \quad (22)$$

Next we consider the limit of a slowly varying potential $V_{\sigma}^{(\text{slow})}$ as been defined before Eq. (12):

$$H^{2\text{DEG}} = -\frac{\hbar^2 \nabla^2}{2m^*} + V_{\sigma}^{(\text{slow})}(\mathbf{r}). \quad (23)$$

If V_{σ} is smaller than $E_{x,\mathbf{k}} (\equiv E_F - \hbar^2 k_y^2 / 2m^*)$, the wave function can be written as

$$\psi_{\sigma,\mathbf{k}}(x, y) = \left(c^{\sigma} e^{i \int_{x_0}^x q_{x,\mathbf{k}}^{\sigma}(x') dx'} + d^{\sigma} e^{-i \int_{x_0}^x q_{x,\mathbf{k}}^{\sigma}(x') dx'} \right) e^{ik_y y}. \quad (24)$$

where $q_{x,\mathbf{k}}^{\sigma}(x') \equiv \sqrt{2m^* (E_F - V_{\sigma}(x'^2 k_y^2 / 2m^*) / \hbar}$ and x_0 is a reference point. In region III

$$\begin{aligned} \psi_{III,\sigma,\mathbf{k}}(x, y) &= t^{\sigma} e^{ik_x x + ik_y y} \\ &= \left(e^{i \int_0^x q_{x,\mathbf{k}}^{\sigma}(x') dx'} + r^{\sigma} e^{-i \int_0^x q_{x,\mathbf{k}}^{\sigma}(x') dx'} \right) e^{ik_y y} \\ &\cong \left(e^{ik_x x + i(q_{x,\mathbf{k}}^{\sigma} - k_x)D} + r^{\sigma} e^{-ik_x x - i(q_{x,\mathbf{k}}^{\sigma} - k_x)D} \right) e^{ik_y y}. \end{aligned} \quad (25)$$

In the semiclassical approximation electrons cannot pass the scattering region when the potential energy is larger than its kinetic energy $E_{x,\mathbf{k}}$. This leads to the transmission and reflection coefficients

$$t_{\mathbf{k}}^{\sigma} = \begin{cases} 0, & E_{x,\mathbf{k}} < V_{\sigma} \\ e^{i(q_{x,\mathbf{k}}^{\sigma} - k_x)D}, & E_{x,\mathbf{k}} > V_{\sigma} \end{cases} \quad (26)$$

$$r_{\mathbf{k}}^{\sigma} = \begin{cases} 1, & E_{x,\mathbf{k}} < V_{\sigma} \\ 0, & E_{x,\mathbf{k}} > V_{\sigma} \end{cases}. \quad (27)$$

where we kept the phase of the transmitted electron waves. Note that the phases accumulated by the adiabatic rise and drop of the potential outside the gate cancel each other.

We display the computed spin current j_s pumped into a 2DEG for an abrupt potential in Fig. 2 (a) and for a slowly varying potential in Fig. 2 (b) as a function of the Fermi energy E_F , the gate voltage V_c , exchange coupling J , and length D . A larger exchange splitting J increases the spin current

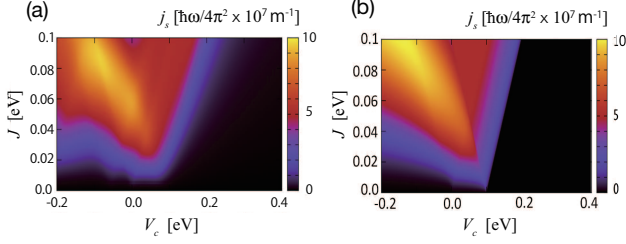


FIG. 2: Spin current per unit width pumped into a 2DEG by an electrically insulating ferromagnetic top contact as a function of the gate voltage V_c and the proximity exchange coupling constant J , assuming that (a) the potential at the contact edges is abrupt and (b) continuous. The chemical potential of the 2DEG $E_F = 0.1$ eV. The transverse length of the top contact is $D = 10$ nm.

pumped into the 2DEG, as expected in the limit of a weak ferromagnet. When $V_\sigma > E_F$, the wave function with spin σ in the limit of an abrupt potential exponentially decays under the FI. The white-dashed line in Fig. 2(a) is the function $V_\uparrow = V_c - J = E_F$. To the far right of it, $V_c \gg E_F$ and j_s vanishes since all electrons are reflected by the high potential barrier. For the slowly varying potentials, electrons are completely reflected when $V_{\uparrow,\downarrow} > E_F$ and j_s vanishes abruptly at the same line as seen in Fig. 2(b). When $V_\sigma < E_F$, electron waves may interfere constructively to maximize the spin current, forming the broad ridge of enhanced spin currents that is observed for both potentials. The black dashed line in Fig. 2(a) is a guide to the eye that coincides with the maximum spin pumping current which occurs when the phase difference between of up spin and down spin electrons becomes large.

In general, we observe that at least for the considered parameter regime, a WKB-like approximation of the spin pumping into the 2DEG that is valid for slowly varying potentials agrees well with the fully quantum mechanical result for abrupt potentials.

B. Graphene

We now turn to spin pumping into graphene, focusing on the \mathbf{K} valley and multiply the result by 2, thereby disregarding intervalley scattering. As before, the electrons in graphene experience the proximity-exchange and electrostatic potentials collected in $U(\mathbf{r}, t)$. We consider the parameter regimes $|E_F|, |V_\sigma| < 1$ eV, for which the standard envelope wave function Hamiltonian with energy zero at the Dirac point applies:

$$H_{kin}^{\text{graphene}} = -i\hbar v_F \hat{\sigma} \cdot \nabla, \quad (28)$$

where $\hat{\sigma} = \sum_l \hat{\sigma}_l \mathbf{e}_l$ and $\hat{\sigma}_l$ ($l = x, y$) are the Pauli matrices in pseudo-spin space. The envelope wave function is the spinor

$$\psi(\mathbf{r}) = \begin{pmatrix} \psi_1(\mathbf{r}) \\ \psi_2(\mathbf{r}) \end{pmatrix}. \quad (29)$$

We discuss again abrupt potentials first:

$$H^{\text{graphene}} = -i\hbar v_F \hat{\sigma} \cdot \nabla + V_\sigma^{\text{(abrupt)}}(\mathbf{r}). \quad (30)$$

In region I ($x < 0$)

$$\psi_{I,\sigma,\mathbf{k}}(\mathbf{r}) = \begin{pmatrix} 1 \\ \chi e^{i\theta_k} \end{pmatrix} e^{ik_x x + ik_y y} + r_{\mathbf{k}}^\sigma \begin{pmatrix} 1 \\ -\chi e^{-i\theta_k} \end{pmatrix} e^{-ik_x x + ik_y y}, \quad (31)$$

while in region II ($0 < x < D$)

$$\psi_{II,\sigma,\mathbf{k}}(\mathbf{r}) = a_{\mathbf{k}}^\sigma \begin{pmatrix} 1 \\ \chi^\sigma e^{i\theta_{q\sigma}} \end{pmatrix} e^{iq_{x,\mathbf{k}}^\sigma x + iq_{y,\sigma} y} + b_{\mathbf{k}}^\sigma \begin{pmatrix} 1 \\ -\chi^\sigma e^{-i\theta_{q\sigma}} \end{pmatrix} e^{-iq_{x,\mathbf{k}}^\sigma x + iq_{y,\sigma} y}, \quad (32)$$

where $q_{x,\mathbf{k}}^\sigma = \sqrt{(E - V_\sigma)^2 / \hbar^2 v_F^2 - k_y^2}$. In region III ($x > D$)

$$\psi_{III,\sigma,\mathbf{k}}(\mathbf{r}) = t_{\mathbf{k}}^\sigma \begin{pmatrix} 1 \\ \chi e^{i\theta_k} \end{pmatrix} e^{ik_x x + ik_y y}, \quad (33)$$

where $\chi = \text{sgn}(E)$, $\chi^\sigma = \text{sgn}(E - V_\sigma)$, $\tan \theta_{\mathbf{k}} = k_y / k_x$, $\tan \theta_{q\sigma} = q_{y,\sigma} / q_{x,\mathbf{k}}^\sigma$. The boundary conditions are $\psi_{I,\sigma}(0, y) = \psi_{II,\sigma}(0, y)$, $\psi_{II,\sigma}(D, y) = \psi_{III,\sigma}(D, y)$ and $k_y = q_{y,\sigma}$. When $|E - V^\sigma| > \hbar v_F |k_y|$ (propagating states in the gated region) transmission and reflection coefficients read

$$t_{\mathbf{k}}^\sigma(\phi) = \frac{e^{-ik_x D} \cos \theta_\sigma \cos \phi}{X_{\mathbf{k}}^\sigma} \quad (34)$$

$$r_{\mathbf{k}}^\sigma(\phi) = \frac{ie^{i\phi} (\chi \chi^\sigma \sin \phi - \sin \theta_\sigma) \sin q_{x,\mathbf{k}}^\sigma D}{X_{\mathbf{k}}^\sigma}, \quad (35)$$

where $X_{\mathbf{k}}^\sigma \equiv \cos \theta_\sigma \cos \phi \cos q_{x,\mathbf{k}}^\sigma D + i(\sin \theta_\sigma \sin \phi - \chi \chi^\sigma) \sin q_{x,\mathbf{k}}^\sigma D$.

When $|E - V^\sigma| < \hbar v_F |k_y|$ (evanescent states in the gated region), we substitute $q_{x,\mathbf{k}}^\sigma = i\kappa_{x,\sigma}$, $e^{i\theta_\sigma} \rightarrow (i\kappa_{x,\sigma} + ik_y) / (|E - V| / \hbar v_F)$ and $-e^{-i\theta_\sigma} \rightarrow (-i\kappa_{x,\sigma} + ik_y) / (|E - V| / \hbar v_F)$ for propagating states. Transmission and reflection coefficients then become

$$t_{\mathbf{k}}^\sigma(\phi) = \frac{i\chi \hbar v_F \kappa_{x,\sigma} \cos \phi e^{-ik_x D \cos \phi}}{Y_{\mathbf{k}}^\sigma} \quad (36)$$

$$r_{\mathbf{k}}^\sigma(\phi) = \frac{-iV_\sigma e^{i\phi} \sinh \kappa_{x,\sigma} D \sin \phi}{Y_{\mathbf{k}}^\sigma}. \quad (37)$$

where $Y_{\mathbf{k}}^\sigma \equiv (E \cos^2 \phi - V_\sigma) \sinh \kappa_{x,\sigma} D + i\chi \hbar v_F \kappa_{x,\sigma} \cos \phi \cosh \kappa_{x,\sigma} D$.

When $E = V_\sigma$, the wave function in region II can be written as

$$\psi_{II,\sigma,\mathbf{k}}(\mathbf{r}) = \begin{pmatrix} A e^{q_y(x+iy)} \\ B e^{\kappa_y(-x+iy)} \end{pmatrix}. \quad (38)$$

With specular scattering boundary condition $q_y = \kappa_y = k_y$:

$$t_{\mathbf{k}}^\sigma(\phi) = \frac{2e^{-ik_y D} \cos \phi}{e^{i\phi} e^{\kappa_y D} + e^{-i\phi} e^{-\kappa_y D}}, \quad (39)$$

$$r_{\mathbf{k}}^\sigma(\phi) = \frac{-2e^{i\phi} \sinh \kappa_y D}{e^{i\phi} e^{\kappa_y D} + e^{-i\phi} e^{-\kappa_y D}}. \quad (40)$$

When $|E| \ll |V_\sigma|$, i.e. the Fermi circle under the gate is much larger than that in the leads, $\cos \theta_\sigma \rightarrow 1$, $\sin \theta_\sigma \rightarrow 0$, and $q_{x,\mathbf{k}}^\sigma \cong |V_\sigma|/\hbar v_F = |V_c \mp J|/\hbar v_F$, leading to the simplified results

$$t_{\mathbf{k}}^\sigma(\phi) \rightarrow \frac{\cos \phi e^{-ik_F D \cos \phi}}{\cos \phi \cos q_{x,\mathbf{k}}^\sigma D - i\chi\chi^\sigma \sin q_{x,\mathbf{k}}^\sigma D}, \quad (41)$$

$$r_{\mathbf{k}}^\sigma(\phi) \rightarrow \frac{i\chi\chi^\sigma e^{i\phi} \sin \phi \sin q_{x,\mathbf{k}}^\sigma D}{\cos \phi \cos q_{x,\mathbf{k}}^\sigma D - i\chi\chi^\sigma \sin q_{x,\mathbf{k}}^\sigma D}. \quad (42)$$

We now turn to a slowly varying potential with Hamiltonian

$$H^{\text{graphene}} = -i\hbar v_F \hat{\sigma} \cdot \nabla + V_\sigma^{\text{(slow)}}(\mathbf{r}). \quad (43)$$

If V_σ is smaller than $E_{x,\mathbf{k}} (\equiv E_F - \hbar v_F |k_y|)$, the wave function can be written as

$$\begin{aligned} \psi_{\sigma,\mathbf{k}}(\mathbf{r}) = & c^\sigma \begin{pmatrix} G_{\sigma,\mathbf{k}}^{-1/2} + iG_{\sigma,\mathbf{k}}^{1/2} k_y/|k_y| \\ G_{\sigma,\mathbf{k}}^{-1/2} - iG_{\sigma,\mathbf{k}}^{1/2} k_y/|k_y| \end{pmatrix} e^{i \int_{x_0}^x q_{x,\mathbf{k}}^\sigma(x') dx' + ik_y y} \\ & + d^\sigma \begin{pmatrix} G_{\sigma,\mathbf{k}}^{1/2} + iG_{\sigma,\mathbf{k}}^{-1/2} k_y/|k_y| \\ G_{\sigma,\mathbf{k}}^{1/2} - iG_{\sigma,\mathbf{k}}^{-1/2} k_y/|k_y| \end{pmatrix} e^{-i \int_{x_0}^x q_{x,\mathbf{k}}^\sigma(x') dx' + ik_y y}, \end{aligned} \quad (44)$$

where x_0 is a reference point, $q_{x,\mathbf{k}}^\sigma = |E_{x,\mathbf{k}} - V_\sigma(x)|/\hbar v_F$, and with $v \equiv \text{sgn}(V_\sigma(x_0) - E)$

$$G_{\sigma,\mathbf{k}} = \left(\frac{|E - V_\sigma(x)|/\hbar v_F + k_x(x)}{|k_y|} \right)^v. \quad (45)$$

In region III:

$$\begin{aligned} \psi_{III,\sigma,\mathbf{k}}(\mathbf{r}) = & t^\sigma \begin{pmatrix} G_{\sigma,\mathbf{k}}^{-1/2} + iG_{\sigma,\mathbf{k}}^{1/2} k_y/|k_y| \\ G_{\sigma,\mathbf{k}}^{-1/2} - iG_{\sigma,\mathbf{k}}^{1/2} k_y/|k_y| \end{pmatrix} e^{ik_x x + ik_y y} \\ = & \begin{pmatrix} G_{\sigma,\mathbf{k}}^{-1/2} + iG_{\sigma,\mathbf{k}}^{1/2} k_y/|k_y| \\ G_{\sigma,\mathbf{k}}^{-1/2} - iG_{\sigma,\mathbf{k}}^{1/2} k_y/|k_y| \end{pmatrix} e^{i \int_{x_0}^x q_{x,\mathbf{k}}^\sigma(x') dx' + ik_y y} \\ & + r^\sigma \begin{pmatrix} G_{\sigma,\mathbf{k}}^{1/2} + iG_{\sigma,\mathbf{k}}^{-1/2} k_y/|k_y| \\ G_{\sigma,\mathbf{k}}^{1/2} - iG_{\sigma,\mathbf{k}}^{-1/2} k_y/|k_y| \end{pmatrix} e^{-i \int_{x_0}^x q_{x,\mathbf{k}}^\sigma(x') dx' + ik_y y} \\ \cong & \begin{pmatrix} G_{\sigma,\mathbf{k}}^{-1/2} + iG_{\sigma,\mathbf{k}}^{1/2} k_y/|k_y| \\ G_{\sigma,\mathbf{k}}^{-1/2} - iG_{\sigma,\mathbf{k}}^{1/2} k_y/|k_y| \end{pmatrix} e^{ik_x x + i(q_{x,\mathbf{k}}^\sigma - k_x)D + ik_y y} \\ & + r^\sigma \begin{pmatrix} G_{\sigma,\mathbf{k}}^{1/2} + iG_{\sigma,\mathbf{k}}^{-1/2} k_y/|k_y| \\ G_{\sigma,\mathbf{k}}^{1/2} - iG_{\sigma,\mathbf{k}}^{-1/2} k_y/|k_y| \end{pmatrix} e^{-ik_x x - i(q_{x,\mathbf{k}}^\sigma - k_x)D + ik_y y}. \end{aligned} \quad (46)$$

In the semiclassical WKB approximation electrons cannot transmit the scattering region when the potential energy is larger than $E_{x,\mathbf{k}}$. This corresponds to disregarding the evanescent wave-tunneling through the gate region. The transport coefficients then read

$$t_{\mathbf{k}}^\sigma = \begin{cases} 0, & E_{x,\mathbf{k}} < V_\sigma \\ e^{i(q_{x,\mathbf{k}}^\sigma - k_x)D}, & E_{x,\mathbf{k}} > V_\sigma \end{cases} \quad (47)$$

$$r_{\mathbf{k}}^\sigma = \begin{cases} 1, & E_{x,\mathbf{k}} < V_\sigma \\ 0, & E_{x,\mathbf{k}} > V_\sigma \end{cases}. \quad (48)$$

where we again preserved the phase of the transmitted electron waves.

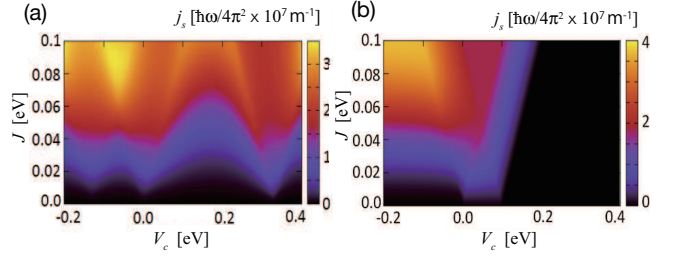


FIG. 3: (a) Spin current per unit width pumped into graphene by a ferromagnetic top layer as a function of the gate voltage V_c and the proximity exchange coupling constant J , assuming that (a) the potential at the contact/gate edges is abrupt and (b) slowly varying. The (zero-bias) chemical potential of the graphene $\mu = 100$ meV. The length of the ferromagnetic region is $D = 10$ nm. $m = 0.9$ is the cosine of the magnetization precession cone angle.

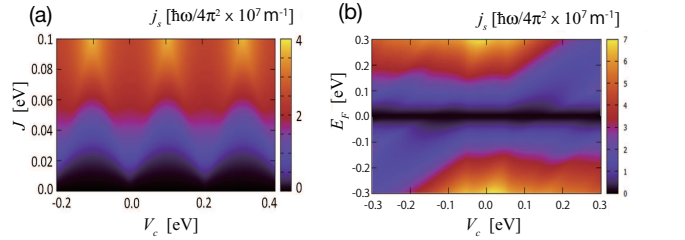


FIG. 4: (a) Spin current per unit width as in Fig. 3 but for $\mu = 1$ meV, i.e. close to the Dirac electron neutrality point. (b) Spin current density pumped into graphene as a function of the (non-adiabatic) gate voltage V_c and Fermi energy of the reservoirs E_F . Other parameters are $J = 50$ meV, gate length $D = 10$ nm, and cosine of the magnetization precession cone angle $m = 0.9$.

We plot the dependence of the spin current density j_s pumped into graphene on V_c and J for an abrupt potential at the contact/gate edges in Fig. 3 (a) and a slowly varying potential in Fig. 3 (b). These figures can be compared with the 2DEG device for the same parameters. In the 2DEG j_s vanishes when $V_\sigma > E_F$ because all electrons are reflected by the potential barrier. On the other hand, in graphene j_s does not vanish even when $V_\sigma > E_F$, because electrons can propagate through the potential by Klein tunneling via the valence band states. In the abrupt potential limit, when $(E_F - V_\sigma)/E_F < -1$ electrons are seen to tunnel efficiently through the gate region. This renders the physics of transport including spin pumping in graphene very different from that of the 2DEG. For the adiabatic potential, however, electrons waves are reflected and Klein tunneling⁴¹ does not occur. Therefore, when $V_\uparrow > E_F$, j_s vanishes.

In Fig. 4(a), we plot j_s for graphene close to electroneutrality ($E_F = 1$ meV), while in Fig. 3 (a) the Fermi energy is substantial. Note that we do not address the complications of transport at the Dirac point (see e.g.⁴²). Since the electron density is very small, the spin pumping spectra in Fig. 4(b) reflect the particle-hole symmetry of the graphene band struc-

ture. The spin current in $n|n(p)\text{-F}|n$ -graphene is the same as that in $p|p(n)\text{-F}|p$ graphene junctions summarized by the general symmetry relation

$$j_s(E_F, V_c) = j_s(-E_F, -V_c) \quad (49)$$

We observe in Fig.4(b) that in the area between the lines $V_c \pm E_F$ the spin current is suppressed because the modes under the gate are evanescent.

III. CONCLUSION

In conclusion, we report spin pumping into a 2DEG and graphene by a planar contact consisting of a magnetic insulator film with a metal gate. In both cases the spin current can be controlled by the gate voltage that modulates the electron density. The pumped spin currents in both systems are remarkably different in the abrupt potential limit, reflecting the difference between the Schrödinger and Dirac equations. Rahimi and Moghaddam²⁹ compute spin pumping into graphene for the same configuration. They do not discuss the 2DEG and focus on different parameter regimes, however. The present theory is valid when the scattering mean-free path is smaller than the system size. We therefore chose a narrow gate with $D = 10$ nm. In contrast to perturbation theory there are no re-

strictions on the magnitude and cone angle of the induced exchange potential. Even for a large $J = 50$ meV, the coherence length is $\lambda \approx 20$ nm, which means that we are in the limit of a weak ferromagnet. We predict typical dependence of the spin current on all device parameters that can be very different for graphene and the 2DEG, mainly by Klein tunneling in the former. The effects can in principle be observed by metallic contacts outside the gated region or enhanced broadening of the ferromagnetic resonance, which requires additional but straightforward modelling of the specific sample.

Future work should take into account disorder scattering, including spin flip scattering, that has been found to be negligible when graphene has a large contact area with a ferromagnet.

Acknowledgments

This work was supported by JSPS KAKENHI Grant Nos. 25247056, 25220910, 26103006, JP26400308, and JP15H05854. G.B. acknowledges the hospitality of the Zernike Institute of the University of Groningen and useful discussions with Bart van Wees and Christian Leutenantsmeyer.

-
- ¹ Y. Ohno, D. K. Young, B. Beschoten, F. Matsukura, H. Ohno, and D. D. Awschalom, *Nature* **402**, 790 (1999).
 - ² F. J. Jedema, A. T. Filip, and B. J. van Wees, *Nature* **410**, 345 (2001).
 - ³ T. Taniyama, E. Wada, M. Itoh, and M. Yamaguchi, *NPG Asia Materials* **3**, 65 (2011).
 - ⁴ K.-R. Jeon, B.-C. Min, S.-Y. Park, K.-D. Lee, H.-S. Song, Y.-H. Park, and S.-C. Shin, *Appl. Phys. Lett.* **103**, 142401 (2013).
 - ⁵ S. Maekawa, H. Adachi, K. Uchida, J. Ieda, and Eiji Saitoh, *J. Phys. Soc. Jpn.* **82**, 102002 (2013).
 - ⁶ A. Brataas, Y. Tserkovnyak, G. E. W. Bauer, and B. I. Halperin, *Phys. Rev. B* **66**, 060404 (2002).
 - ⁷ Q. Wu, L. Shen, Z. Bai, M. Zeng, M. Yang, Z. Huang, and Y. P. Feng, *Phys. Rev. Appl.* **2**, 044008 (2014).
 - ⁸ K. Uchida, J. Xiao, H. Adachi, J. Ohe, S. Takahashi, J. Ieda, T. Ota, Y. Kajiwara, H. Umezawa, H. Kawai, G. E. W. Bauer, S. Maekawa & E. Saitoh, *Nature Mat.* **9**, 894 (2010).
 - ⁹ V. Umansky, R. de-Picciotto, and M. Heiblum, *Appl. Phys. Lett.* **71**, 683 (1997).
 - ¹⁰ X. Lou, C. Adelman, S. A. Crooker, E. S. Garlid, J. Zhang, S. M. Reddy, S. D. Flexner, C. J. Palmstrom, and P. A. Crowell, *Nature Physics* **3**, 197 (2007).
 - ¹¹ M. I. Katsnelson, K. S. Novoselov, and A.K. Geim, *Nat. Phys.* **2**, 620 (2006).
 - ¹² R. Ohshima, A. Sakai, Y. Ando, T. Shinjo, K. Kawahara, H. Ago, and M. Shiraishi, *Appl. Phys. Lett.* **105**, 162410 (2014).
 - ¹³ Z. Tang, E. Shikoh, H. Ago, K. Kawahara, Y. Ando, T. Shinjo, and M. Shiraishi, *Phys. Rev. B* **87**, 140401(R) (2013).
 - ¹⁴ H. Li, J. Shao, D. Yao, and G. Yang, *ACS Appl. Mater. Interfaces* **6** 1759 (2014).
 - ¹⁵ A. K. Geim, and K. S. Novoselov, *Nat. Mat.* **6** 184 (2007).
 - ¹⁶ W. Han, R. K. Kawakami, M. Gmitra, and J. Fabian, *Nature Nanotech.* **9**, 794 (2014).
 - ¹⁷ J. B. S. Mendes, O. Alves Santos, L. M. Meireles, R. G. Lacerda, L. H. Vilela-Leao, F. L. A. Machado, R. L. Rodriguez-Suarez, A. Azevedo, and S. M. Rezende, *Phys. Rev. Lett.* **115**, 226601 (2015).
 - ¹⁸ Marc Drogeler, Christopher Rranzen, Frank Volmer, Tobias Pohlmann, Luca Banszerus, Maik Wolter, Kenji Watanabe, Takashi Taniguchi, Christoph Stampfer, and Bernd Beschoten, *Nano Lett.* **16**, 3533 (2016).
 - ¹⁹ L. Banszerus, M. Schmitz, S. Engels, J. Dauber, M. Oellers, F. Haupt, K. Watanabe, T. Taniguchi, B. Beschoten, and C. Stampfer, *Science Adv.* **1**, e1500222 (2015).
 - ²⁰ J. Ingla-Aynés, M. H. D. Guimarães, R. J. Meijerink, P. J. Zomer, and B. J. van Wees, *Phys. Rev. B* **92**, 201410R (2015).
 - ²¹ A. H. C. Neto, F. Guinea, N. M. R. Peres, K. S. Novoselov, and A.K. Geim, *Rev. Mod. Phys.* **81**, 109 (2009).
 - ²² A. K. Patra, S. Singh, B. Barin, Y. Lee, J.-H. Ahn, E. del Barco, E. R. Mucciolo, and B. Özyilmaz, *Appl. Phys. Lett.* **101**, 162407 (2012).
 - ²³ S. Singh, A. K. Patra, B. Barin, E. del Barco, and B. Özyilmaz, *IEEE Trans. Magn.* **49**, 3147 (2013).
 - ²⁴ Y. Tserkovnyak, A. Brataas, G. E. W. Bauer, and B. I. Halperin, *Rev. Mod. Phys.* **77**, 1375 (2005).
 - ²⁵ Y. Tserkovnyak, A. Brataas, and G. E. W. Bauer, *Phys. Rev. Lett.* **88**, 117601 (2002).
 - ²⁶ Y. Tserkovnyak, A. Brataas, and G. E. W. Bauer, *Phys. Rev. B* **66**, 224403 (2002).
 - ²⁷ S. Mizukami, Y. Ando, and T. Miyazaki, *Phys. Rev. B* **66**, 104413 (2002); *J. Magn. Magn. Mater.* **239**, 42 (2002).
 - ²⁸ P. W. Brouwer, *Phys. Rev. B* **58**, R10135 (1998).

- ²⁹ M. A. Rahimi and A. G. Moghaddam, J. Phys. D: Appl. Phys. **48** 295004 (2014).
- ³⁰ Z. Wang, C. Tang, R. Sachs, Y. Barlas, J. Shi, Phys. Rev. Lett. **114**, 016603 (2015).
- ³¹ J.C. Leutenantsmeyer, A.A. Kaverzin, M. Wojtaszek, and B.J. van Wees, arXiv:1601.00995.
- ³² H. X. Yang, A. Halla, D. Terrade, X. Waintal, S. Roche, and M. Chshiev, Phys. Rev. Lett. **110**, 046603 (2013).
- ³³ P. Wei., S. Lee, F. Lemaitre, L. Pinel, D. Cutaia, W. Cha, F. Katmis, Y. Zhu, D. Heiman, J. Hone, J. S. Moodera, and C. Chen, Nat. Mat. **15**, 711 (2016).
- ³⁴ S. M. Watts, J. Grollier, C. H. van der Wal, and B. J. van Wees, Phys. Rev. Lett. **96**, 077201 (2006).
- ³⁵ S. M. Watts and B. J. van Wees, Phys. Rev. Lett. **97**, 116601 (2006).
- ³⁶ J. P. McGuire, C. Ciuti, and L. J. Sham, Phys. Rev. B **69**, 115339 (2004)
- ³⁷ Z. Wang, C. Tang, R. Sachs, Y. Barlas, and J. Shi, Phys. Rev. Lett. **114**, 016603 (2015).
- ³⁸ H. Haugen, D. H.-Hernando, and A. Brataas, Rhys. Rev. B **77**, 115406 (2008).
- ³⁹ T. Yokoyama, Phys. Rev. B **77**, 073413 (2008).
- ⁴⁰ E. Saitoh, M. Ueda, H. Miyajima, and G. Tatara, Appl. Phys. Lett. **88**, 182509 (2006).
- ⁴¹ K. J. A. Reijnders, T. Tudorovskiy, and M. I. Katsnelson, Ann. Phys. **333**, 155 (2013).
- ⁴² J.-H. Chen, C. Jang, S. Adam, M. S. Fuhrer, E. D. Williams, and M. Ishigami, Nat. Phys. **4**, 377 (2008)
- ⁴³ B. Dlubak, M-B Martin, C. Deranlot, B. Servet, S. Xavier, R. Mattana, M. Sprinkle, C. Berger, W. A. D. Heer, F. Petroff, A. Anane, P. Seneor, and A. Fert, Nat. Phys. **8**, 557 (2012)